

Trivial and topological bound states in bilayer graphene quantum dots and rings

Nassima Bachtaber,¹ David Sánchez,^{1,2} and Llorenç Serra^{1,2}

¹*Institute for Cross-Disciplinary Physics and Complex Systems IFISC (CSIC-UIB), E-07122 Palma, Spain*

²*Department of Physics, University of the Balearic Islands, E-07122 Palma, Spain*

We discuss and compare two different types of confinement in bilayer graphene by top and bottom gating with symmetrical microelectrodes. Trivial confinement corresponds to the same polarity of all top gates, which is opposed to that of all bottom ones. Topological confinement requires the polarity of part of the top-bottom pairs of gates to be reversed. We show that the main qualitative difference between trivial and topological bound states manifests itself in the magnetic field dependence. We illustrate our finding with an explicit calculation of the energy spectrum for quantum dots and rings. Trivial confinement shows bunching of levels into degenerate Landau bands, with a non-centered gap, while topological confinement shows no field-induced gap and a sequence of state branches always crossing zero-energy.

I. INTRODUCTION

The topological nature of bound states is a research question of ongoing interest^{1,2}. Partly due to the many applications that these states might have for quantum computation³, it is crucial to propose reliable tests that help differentiate between bound states arising from trivial confinement and those arising from topological confinement. The latter show more robustness against weak disorder but it is not easy to detect their presence⁴, which is a prerequisite for their subsequent manipulation and measurement in topological quantum information tasks.

Bilayer graphene (BLG)⁵ in a Bernal stacking structure is a especially suitable platform for creating solid-state electronic qubits due to its long decoherence times⁶. Confinement in BLG is achieved by means of a pair of gates applied to the graphene sheets. In this manner, an energy gap opens around the Fermi level, which is the building block for tunnel barriers^{7,8}. The only requirement is that the potential applied to a sheet has the sign opposite to that of the second sheet. This mechanism has been proven successfully in the recent years when serially connecting tunnel barriers^{9–12}. This confinement is dubbed trivial because the electronic wave functions vanish asymptotically deep in the barriers. Calculations of trivial dots and rings can be found, e.g., in Refs. 13–18.

A totally different confinement mechanism arises when the gate potential changes sign on the same sheet (with the corresponding sign reversal on the second sheet)¹⁹. This can be done with inhomogeneous potentials such as those occurring across a domain wall. As a consequence, there appear kink electronic states (two per valley) bounded along the wall. They are topological because their motion is along the edge and exhibit valley-momentum locking^{19–21}. When the wall forms a closed loop, one can create quantum dots and rings supporting topological bound states^{22,23}. In this paper, we show that these states could be unambiguously detected by examining their behavior with an external magnetic field, which allows us to distinguish between both (trivial and topological) binding mechanisms.

Figure 1 shows a sketch of a BLG system with top-

bottom gating defining circular nanostructures. The distribution of gates is symmetric, i.e., the same for top and bottom sheets while the applied potentials V_a on the top gates is sign reversed with respect to the bottom gates. This way, a potential difference is created between the two graphene layers sandwiched by a given pair of top-bottom gates. Due to the proximity of both graphene layers, much smaller than the gates separation, the effective interlayer field will be smaller than the inter-gate field, but it may be tuned in a proportional way.

We call *trivial confinement* the case when all gates on a given side of the BLG planes, top or bottom, have the same sign. This corresponds to an electric field always in the same direction across the BLG planes, say upwards, confinement being caused by the preference of electrons to attach to the regions of low or vanishing electric field.

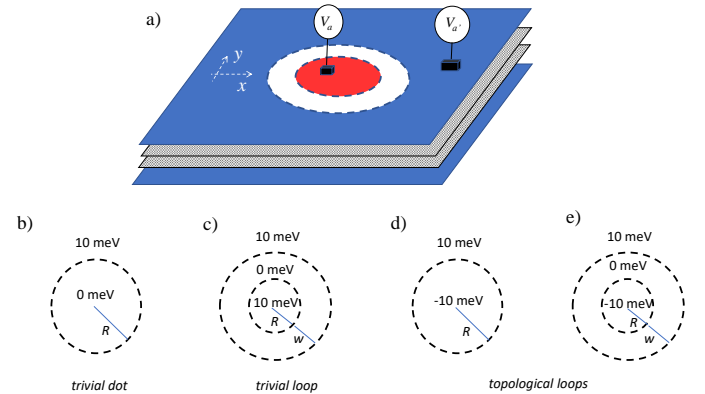


FIG. 1. a) Generic distribution of top-bottom gate pairs inducing the formation of bound states in BLG. Only the top gates are shown (red and blue), with a similar distribution of bottom gates hidden under the two graphene layers (gray planes). The potentials V_a , V'_a are reversed in the bottom gates. b)-e) Selected configurations for bound states in BLG nanostructures induced by the indicated gate potentials: trivial dot of radius R (b), trivial ring of radius R and width w (c), and topological rings of radius R with vanishing width (d) and finite width w (e).

This is indicated by the white region in Fig. 1a, and in the 0 meV region of Fig. 1b (trivial dot) and Fig. 1c (trivial ring).

Topological confinement requires gates on a given side, top or bottom, to have potentials of different signs. This way, the BLG interlayer field changes direction creating a topological domain wall able to bind electrons. Figure 1d sketches the situation of a topological circular ring. It would correspond to the top gates of blue and red color in Fig. 1a having potentials 10 meV and -10 meV, respectively, with a sign change in the white region. We also stress that, differently to the trivial confinement, the topological confinement does not require an extended region of vanishing field; even an abrupt domain wall Fig. 1d creates bound states. This is already indicating the predominantly 1d character of topological states in BLG, as opposed to the predominantly 2d character of the trivial confinement. As shown below, this results in conspicuous physical differences regarding the spectrum dependence on magnetic field.

We can now present the main finding of this work. In the presence of a perpendicular magnetic field, trivial confinement spectra show a bunching of levels indicating the emergence of the 2d physics of Landau levels in BLG. The larger the 2d region of trivial states, the smaller the field at which Landau-level bunching is observed. At zero field there is a finite-size spectrum discretization that evolves as a function of the field into the mentioned level bunching and the formation of a gap for energies in $[0, \sqrt{2}\hbar\omega_c]$, where ω_c is the BLG intrinsic cyclotron energy defined below. Quite differently, topological structures like those in Fig. 1d,e do not show the formation of a gap with magnetic field, but a periodic repetition of continuum branches crossing zero energy. Below, we provide quantitative comparisons of the magnetic energy spectra of BLG trivial and topological confinements, emphasizing the differences between both types. These comparisons are based on numerical calculations that use radial grids with small spacings, allowing high precision for circular dots and rings. In some cases we also consider 2d grid calculations, only to confirm the physical scenario for systems departing from circular symmetry.

II. MODEL

We consider a 2d (xy) continuum model for the low-energy excitations of BLG, already used in our previous works,^{21,23} and also by many other authors (see Refs. 5 and 24 for reviews). The Hamiltonian reads

$$H = v_F \left(p_x - \hbar \frac{y}{2l_z^2} \right) \tau_z \sigma_x + v_F \left(p_y + \hbar \frac{x}{2l_z^2} \right) \sigma_y + \frac{t}{2} (\lambda_x \sigma_x + \lambda_y \sigma_y) + V_a(x, y) \lambda_z, \quad (1)$$

Here, $\hbar v_F = 660$ meV nm and $t = 380$ meV are the Fermi velocity and interlayer coupling, respectively, which are

BLG intrinsic parameters. The sublattice, layer and valley two-fold discrete degrees of freedom of BLG are represented by the $\sigma_{x,y,z}$, $\lambda_{x,y,z}$ and $\tau_{x,y,z}$ sets of Pauli matrices, respectively. The influence of a vertical magnetic field B is included by means of the magnetic length parameter $l_z = \sqrt{\hbar/eB}$, in a symmetric gauge affecting the p_x and p_y operators. Notice that H contains only linear momentum terms, a characteristic of Dirac or relativistic-like Hamiltonians.

A remarkable property of BLG is that confinement to nanostructures can be achieved with the Hamiltonian of Eq. (1) by space modulation of the layer-asymmetry potential $V_a(x, y)$. This is a potential imbalance between the two graphene layers that can be tuned by top and bottom gating, as sketched in Fig. 1. Physically, the electrons have a preference to stay in regions where this potential imbalance is lower and this can be exploited to confine them in nanostructures whose shape is controlled by the shape of the gates. A simplest geometry of confinement that has attracted much attention is the circularly symmetric shape, both as quantum dots and rings. Noncircular shapes have been discussed in Ref. 23.

In this work we consider a layer-asymmetry potential of circular shape, parameterized as

$$V_a(r) = V_a^{(in)} \frac{1}{1 + e^{(r-R)/s}} + V_a^{(out)} \left(1 - \frac{1}{1 + e^{(r-R-w)/s}} \right), \quad (2)$$

where $V_a^{(in)}$ represents an inner saturation value for $r < R$ and $V_a^{(out)}$ an outer saturation value for $r > R+w$. The potential $V_a(r)$ is vanishing for $r \in [R, R+w]$ and s is a small diffusivity suggested by realistic electrostatic simulations of straight kinks,²⁵ which is also convenient for numerical stability. Appropriately choosing parameters R , w and $V_a^{(in,out)}$ it is possible to model the different types of confinements sketched in Fig. 1. These radial potentials can be created by disk-like microelectrodes, as suggested in Fig. 1.

As mentioned in Sec. I, the aim of this work is to compare two qualitatively different types of confinement in BLG: trivial confinement corresponding to saturation potentials of the same sign, $\text{sgn}(V_a^{(in)}) = \text{sgn}(V_a^{(out)})$, and topological confinement corresponding to saturation potentials of different signs, $\text{sgn}(V_a^{(in)}) \neq \text{sgn}(V_a^{(out)})$. Our parameterization allows a flexible modelling of trivial dots and rings. It also allows us to describe topological rings of zero or finite widths. Previous works have investigated trivial dots and rings as well as topological rings, but the latter only with $w = 0$.^{22,23} Here we will also explore the case of a topological ring with a finite w , where potential $V_a(r)$ vanishes and the electrons are essentially free to move.

In presence of a vertical magnetic field electron states in bulk BLG, with $V_a(r) = 0$, are characterized by the

emergence of discrete Landau levels with energies⁵

$$\begin{cases} E_0 = 0, \\ E_1 = 0, \\ E_{\ell,\pm} = \pm \hbar \omega_c \sqrt{\ell(\ell-1)}, \quad \ell = 2, 3, 4, \dots \end{cases} \quad (3)$$

There exists a two-fold degenerate Landau level at zero energy and a sequence of field-dispersing levels at both positive and negative energies. The cyclotron frequency in Eq. (3) is $\omega_c = eB/m_0$, with a mass parameter given by the BLG intrinsic parameters, $m_0 = t/2v_F^2$. The spectrum of Eq. (3) is degenerate for both valleys.

In finite structures like those in Fig. 1 we can expect the emergence of Landau levels for high enough fields provided that the system contains a 2d-like region, i.e., a region with $V_a = 0$ where locally electron motion is free and the system resembles bulk BLG. We will show below that, indeed, our calculations indicate Landau level formation in trivial dots (Fig.1b), trivial rings (Fig.1c) and topological rings of finite width (Fig.1e), but not in topological rings of vanishing width (Fig.1d). The latter only contain 1d-like loop states, whose energies show B -periodic repetitions of linearly dispersing branches reflecting the Aharonov-Bohm periodicities in the flux piercing the loop.

A practical advantage of the circular symmetry is that we can define subspaces of fixed angular momentum m , performing independent diagonalizations in each m subspace. Notice, first, that valley subspaces are always independent in the Hamiltonian of Eq. (1), irrespectively of the spatial circular or noncircular symmetry. We can then assume $\tau_z \equiv 1$, with the reversed valley $\tau_z \equiv -1$ eigenvalues being given by symmetry arguments reversing the energy signs of the $\tau_z \equiv 1$ eigenvalues. In the remaining sublattice and layer subspaces, the spatial wave function for angular momentum m can be written as a 4 component spinor

$$\begin{pmatrix} e^{i(m-1)\theta} C_1(r) \\ e^{im\theta} C_2(r) \\ e^{im\theta} C_3(r) \\ e^{i(m+1)\theta} C_4(r) \end{pmatrix} \quad (4)$$

with (r, θ) the polar coordinates.

It can be shown that, with the spinor wave function of Eq. (4) and Hamiltonian H of Eq. (1), one can fully remove the θ -dependencies and diagonalize a purely radial Hamiltonian $H_m(r, p_r)$ for each angular momentum m ,

$$\begin{aligned} H_m(r, p_r) &= v_F p_r \sigma_x \\ &+ \hbar v_F \left(\frac{m}{r} + \frac{r}{2l_z^2} \right) \sigma_y - \hbar v_F \frac{1}{2r} \sigma_y \lambda_z \\ &+ \frac{t}{2} (\lambda_x \sigma_x + \lambda_y \sigma_y) + V_a(r) \lambda_z, \end{aligned} \quad (5)$$

with $p_r = -i\hbar d/dr$ the radial momentum.

Hamiltonian H_m can be diagonalized for a given layer-asymmetry potential $V_a(r)$ using finite differences in a radial grid and imposing the zero condition at the boundaries. Notice that with $m \neq 0$ there is a $1/r$ divergence at

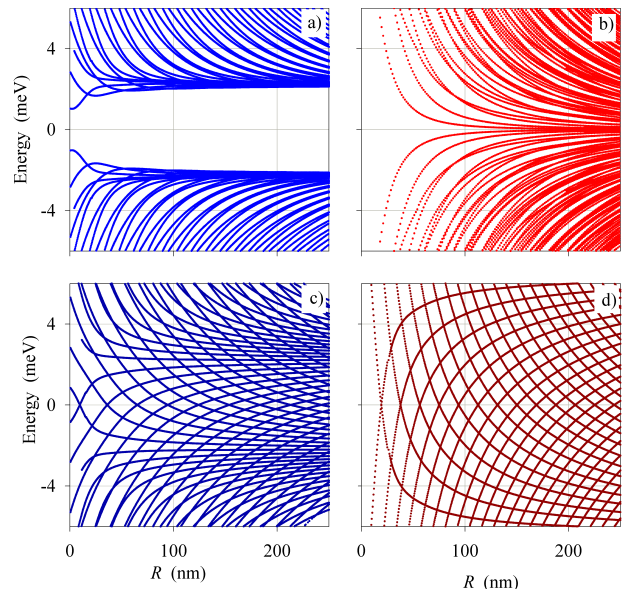


FIG. 2. Spectrum of eigenvalues with vanishing magnetic field. (a) Trivial ring, $V_a^{(in)} = V_a^{(out)} = 10$ meV, $w = 50$ nm; (b) trivial dot, $V_a^{(in)} = 0$, $V_a^{(out)} = 10$ meV, $w = 0$; (c) topological ring $V_a^{(in)} = -V_a^{(out)} = -10$ meV, $w = 50$ nm; (d) topological ring $V_a^{(in)} = -V_a^{(out)} = -10$ meV, $w = 0$. In all cases we used $s = 2.5$ nm.

the origin in Eq. (5), which is compensated by the behavior of the wave function. Numerically, this is more easily taken into account by including a finite value of R (even if quite small) as in trivial and topological rings. An important aspect to bear in mind in the grid diagonalization of Eq. (5) is the possible appearance of spurious solutions due to the known-problem of Fermion doubling for Dirac Hamiltonians. We have carefully considered this, filtering out spurious solutions by defining grid-average wave functions and eliminating those solutions whose norm is affected by such grid averaging.²¹ As mentioned in Sec. I, we have also performed in some test cases the diagonalization of the Hamiltonian given by Eq. (1) without separating in subspaces of angular momentum. However, this is much more demanding computationally and we have only checked the agreement of both methods in a few selected cases.

III. RESULTS

Figure 2 presents selected results for trivial and topological circular systems as a function of size, in zero magnetic field. Notice that we associate the trivial or topological character to the type of confinement and, therefore, this character is shared by the whole low-energy spectrum of eigenstates associated with that particular type of confinement. A trivial ring (Fig. 2a) is characterized by a conspicuous gap in the spectrum around zero en-

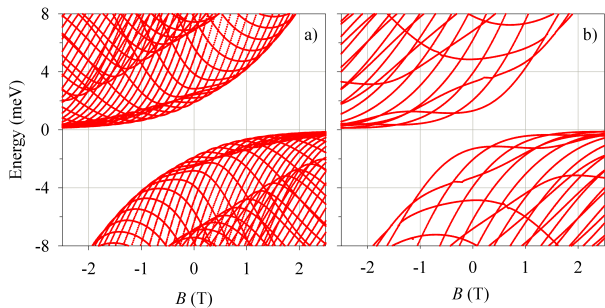


FIG. 3. Spectra as a function of perpendicular magnetic field of trivial rings (Fig. 1c) with (a) $R = 50$ nm, $w = 50$ nm; (b) $R = 10$ nm, $w = 50$ nm. Panel (b) is similar to a trivial dot. We used the same $V_a^{(in)}$, $V_a^{(out)}$ and s of Fig. 2.

ergy, due to the energy quantization induced by the finite w . In trivial dots or rings with smaller w 's this energy gap is much reduced or totally closed for large values of the radius (Fig. 2b). In sharp contrast, the topological systems present a qualitatively different behavior (Fig. 2cd). Intersecting energy branches of positive and negative slopes, always crossing zero energy are the main characteristic of the topological systems. In $w = 0$ topological loops (Fig. 2d) the pattern of crossings is very regular and, as discussed in Ref. 23, can be explained with a quantization rule for 1d closed orbits, similar to the Bohr-Sommerfeld one. The topological ring of finite width (Fig. 2c) presents a remarkable behavior, simultaneously showing the zero energy intersecting branches and also a merging of horizontal branches at energies $\approx \pm 2$ meV, clearly reminiscent of the gap in a trivial ring of the same size (Fig. 2a).

We consider next the role of a perpendicular magnetic field. As discussed above, in systems with regions of 2d electronic motion there is a competition of finite size and B -field discretization into Landau levels; the latter being eventually dominant for large enough fields. Figures 3a and 3b show the results for trivial rings with a large and a small width w , respectively; the latter resembling a quantum dot. Figure 3 is for one valley ($\tau_z = +1$), with the spectrum for the complementary valley ($\tau_z = -1$) being given by reversing the energy signs. The energy states have an exact symmetry by inversion of both magnetic field and valley. This implies complete valley degeneracy at zero field, which is the time-reversal-invariant limit. The most noticeable feature in Fig. 3 is the evolution of the energy gap position. Zero energy is the gap center for $B = 0$ but it evolves into a gap edge at large fields. This is a clear indication of Landau band discretization. For instance, with positive magnetic fields the bulk Landau gap $[0, \sqrt{2}\hbar\omega_c]$ at 1.5 T is $[0, 7.5$ meV], in good qualitative agreement with the results of Fig. 3. This figure also shows how for the same value of w the spectrum of a ring with a larger R contains more bands and a cleaner merging into Landau levels at large fields.

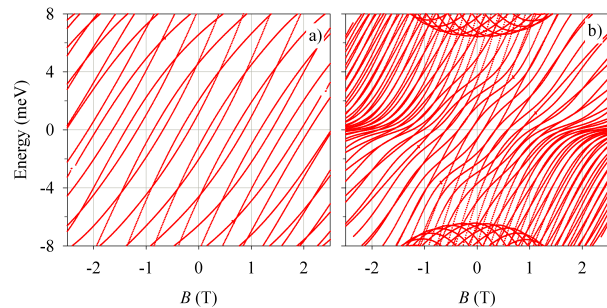


FIG. 4. Spectra of topological rings (Fig. 1d,e) with (a) $R = 50$ nm, $w = 0$ nm; (b) $R = 50$ nm, $w = 50$ nm. We used the same $V_a^{(in)}$, $V_a^{(out)}$ and s of Fig. 2.

The spectra for topological systems in magnetic field are shown in Fig. 4. As anticipated in Sec. I, the topological loop of zero width (Fig. 4a) shows no signs of Landau level physics. Instead, its level spectrum is a sequence of almost parallel branches with similar B -slopes. Figure 4 is for one valley, the reversed valley having similar branches but with the opposite B -slopes. The case of a topological loop of finite width (Fig. 4b) is again most remarkable (as in Fig. 2c), showing the mentioned almost parallel branches and, also, signatures of Landau level discretization. The latter is hinted by the level bunching around zero energy for large (positive and negative) fields, as well as by the new branches emerging at large (positive and negative) energies in Fig. 4b.

IV. DISCUSSION AND CONCLUSIONS

We have discussed two types of confinement in BLG nanostructures induced by top and bottom gating. Trivial and topological confinement differ in the potential signs applied to the gates. The regions with zero layer-asymmetry potential correspond to locally free electronic motion.

Confronting Figs. 3 and 4 we observe the sharp differences in the eigenvalue spectra of trivial and topological systems. The B -increasing gap (for a given valley), with one gap edge pinned at $E = 0$, is a characteristic that permits to intrinsically differentiate trivial and topological states in BLG systems. Landau level physics requires a 2d region of vanishing layer-asymmetry potential, where electron motion is locally free. On the contrary, topological rings of vanishing width behave as purely 1d loops and do not show signatures of Landau level formation. Instead, they manifest B -periodicities indicating Aharonov-Bohm physics reminiscent of the flux periodicities of rings built with metals or semiconductor 2d electron gases.

At $B = 0$ trivial rings and dots have an energy gap centered around zero energy, larger for the case of rings than for dots. Switching on a magnetic field, this gap

evolves into the mentioned non-centered gap of Landau level physics. Quite remarkably, topological rings of finite width manifest both Aharonov-Bohm periodicities and signatures of Landau level discretization in magnetic field.

Our numerical estimates suggest that the magnetic spectrum of both confinement types could be detected using today's experimental techniques, which would represent a significant step toward topological quantum computation in graphene systems.

ACKNOWLEDGMENTS

We acknowledge support from AEI (Spain) Grant No. PID2020-117347GB-I00, MINECO/AEI/FEDER María de Maeztu Program for Units of Excellence MDM2017-0711, and GOIB Grant No. PDR2020-12.

-
- ¹ Liang Fu and C. L. Kane, "Superconducting proximity effect and majorana fermions at the surface of a topological insulator," *Phys. Rev. Lett.* **100**, 096407 (2008).
 - ² Takuya Kitagawa, Matthew A. Broome, Alessandro Fedrizzi, Mark S. Rudner, Erez Berg, Ivan Kassal, Alán Aspuru-Guzik, Eugene Demler, and Andrew G. White, "Observation of topologically protected bound states in photonic quantum walks," *Nature Communications* **3**, 882 (2012).
 - ³ Chetan Nayak, Steven H. Simon, Ady Stern, Michael Freedman, and Sankar Das Sarma, "Non-abelian anyons and topological quantum computation," *Rev. Mod. Phys.* **80**, 1083–1159 (2008).
 - ⁴ Michael Schüler, Umberto De Giovannini, Hannes Hübener, Angel Rubio, Michael A. Sentef, Thomas P. Devereaux, and Philipp Werner, "How circular dichroism in time- and angle-resolved photoemission can be used to spectroscopically detect transient topological states in graphene," *Phys. Rev. X* **10**, 041013 (2020).
 - ⁵ Edward McCann and Mikito Koshino, "The electronic properties of bilayer graphene," *Reports on Progress in Physics* **76**, 056503 (2013).
 - ⁶ Björn Trauzettel, Denis V. Bulaev, Daniel Loss, and Guido Burkard, "Spin qubits in graphene quantum dots," *Nature Physics* **3**, 192–196 (2007).
 - ⁷ Hiske Overweg, Angelika Knothe, Thomas Fabian, Lukas Linhart, Peter Rickhaus, Lucien Wernli, Kenji Watanabe, Takashi Taniguchi, David Sánchez, Joachim Burgdörfer, Florian Libisch, Vladimir I. Fal'ko, Klaus Ensslin, and Thomas Ihn, "Topologically nontrivial valley states in bilayer graphene quantum point contacts," *Phys. Rev. Lett.* **121**, 257702 (2018).
 - ⁸ R. Kraft, I. V. Krainov, V. Gall, A. P. Dmitriev, R. Krupke, I. V. Gornyi, and R. Danneau, "Valley subband splitting in bilayer graphene quantum point contacts," *Phys. Rev. Lett.* **121**, 257703 (2018).
 - ⁹ Marius Eich, F. Herman, Riccardo Pisoni, Hiske Overweg, Annika Kurzmann, Yongjin Lee, Peter Rickhaus, Kenji Watanabe, Takashi Taniguchi, Manfred Sigrist, Thomas Ihn, and Klaus Ensslin, "Spin and valley states in gate-defined bilayer graphene quantum dots," *Phys. Rev. X* **8**, 031023 (2018).
 - ¹⁰ Annika Kurzmann, Hiske Overweg, Marius Eich, Alessia Pally, Peter Rickhaus, Riccardo Pisoni, Yongjin Lee, Kenji Watanabe, Takashi Taniguchi, Thomas Ihn, and Klaus Ensslin, "Charge detection in gate-defined bilayer graphene quantum dots," *Nano Letters* **19**, 5216–5221 (2019).
 - ¹¹ L. Banszerus, A. Rothstein, T. Fabian, S. Möller, E. Icking, S. Trellenkamp, F. Lentz, D. Neumaier, K. Watanabe, T. Taniguchi, F. Libisch, C. Volk, and C. Stampfer, "Electron hole crossover in gate-controlled bilayer graphene quantum dots," *Nano Letters* **20**, 7709–7715 (2020).
 - ¹² L. Banszerus, K. Hecker, E. Icking, S. Trellenkamp, F. Lentz, D. Neumaier, K. Watanabe, T. Taniguchi, C. Volk, and C. Stampfer, "Pulsed-gate spectroscopy of single-electron spin states in bilayer graphene quantum dots," *Phys. Rev. B* **103**, L081404 (2021).
 - ¹³ J. Milton Pereira, P. Vasilopoulos, and F. M. Peeters, "Tunable quantum dots in bilayer graphene," *Nano Letters* **7**, 946–949 (2007).
 - ¹⁴ Patrik Recher, Johan Nilsson, Guido Burkard, and Björn Trauzettel, "Bound states and magnetic field induced valley splitting in gate-tunable graphene quantum dots," *Phys. Rev. B* **79**, 085407 (2009).
 - ¹⁵ M. Zarenia, J. M. Pereira, F. M. Peeters, and G. A. Farias, "Electrostatically confined quantum rings in bilayer graphene," *Nano Letters* **9**, 4088–4092 (2009).
 - ¹⁶ J. M. Pereira, F. M. Peeters, P. Vasilopoulos, R. N. Costa Filho, and G. A. Farias, "Landau levels in graphene bilayer quantum dots," *Phys. Rev. B* **79**, 195403 (2009).
 - ¹⁷ M. Zarenia, J. Milton Pereira, A. Chaves, F. M. Peeters, and G. A. Farias, "Simplified model for the energy levels of quantum rings in single layer and bilayer graphene," *Phys. Rev. B* **81**, 045431 (2010).
 - ¹⁸ M. Zarenia, J. Milton Pereira, A. Chaves, F. M. Peeters, and G. A. Farias, "Erratum: Simplified model for the energy levels of quantum rings in single layer and bilayer graphene [phys. rev. b 81, 045431 (2010)]," *Phys. Rev. B* **82**, 119906 (2010).
 - ¹⁹ Ivar Martin, Ya. M. Blanter, and A. F. Morpurgo, "Topological confinement in bilayer graphene," *Phys. Rev. Lett.* **100**, 036804 (2008).
 - ²⁰ M. Zarenia, J. M. Pereira, G. A. Farias, and F. M. Peeters, "Chiral states in bilayer graphene: Magnetic field dependence and gap opening," *Phys. Rev. B* **84**, 125451 (2011).
 - ²¹ Nassima Benchtaber, David Sánchez, and Llorenç Serra, "Scattering of topological kink-antikink states in bilayer graphene structures," *Phys. Rev. B* **104**, 155303 (2021).
 - ²² L. J. P. Xavier, J. M. Pereira, Andrey Chaves, G. A. Farias, and F. M. Peeters, "Topological confinement in graphene bilayer quantum rings," *Applied Physics Letters* **96**, 212108 (2010).
 - ²³ Nassima Benchtaber, David Sánchez, and Llorenç Serra, "Geometry effects in topologically confined bilayer graphene loops," *New Journal of Physics* **24**, 013001 (2021).

- ²⁴ A.V. Rozhkov, A.O. Sboychakov, A.L. Rakhmanov, and Franco Nori, “Electronic properties of graphene-based bilayer systems,” *Physics Reports* **648**, 1–104 (2016), electronic properties of graphene-based bilayer systems.
- ²⁵ Jing Li, Ke Wang, Kenton J. McFaul, Zachary Zern, Yafei Ren, Kenji Watanabe, Takashi Taniguchi, Zhenhua Qiao, and Jun Zhu, “Gate-controlled topological conducting channels in bilayer graphene,” *Nature Nanotechnology* **11**, 1060–1065 (2016).